ADVANCED OPTICAL MATERIALS
www.advopticalmat.de

The Role of Porosity in SERS

Miguel A. Correa-Duarte, I. Brian Becerril-Castro, and Ramon A. Alvarez-Puebla**

Porosity serves as a critical design parameter in advancing surface-enhanced Raman scattering (SERS) spectroscopy by simultaneously addressing two fundamental challenges: analyte concentration and electromagnetic field enhancement. This review systematically examines how precisely engineered porous architectures including intrinsic nanoporous metals, functional polymer matrices, mesoporous silica hybrids, and crystalline metal-organic frameworks (MOFs), create synergistic platforms that significantly boost SERS performance. The unique pore structures of these materials provide three key advantages: 1) enhanced molecular enrichment near plasmonic surfaces through size-selective trapping, 2) increased density of electromagnetic hotspots via nanoscale cavity engineering, and 3) improved substrate stability and reusability.

1. Introduction

Surface-enhanced Raman scattering (SERS) spectroscopy is a powerful analytical technique that significantly amplifies the Raman scattering signal of molecules adsorbed on metallic nanostructures, enabling the detection of ultralow-concentrations of analytes.[1] Over the last 50 years, SERS has undergone transformative advancements, not only in the development of instrumental techniques (i.e., surface-enhanced hyper-Raman scattering (SEHRS) spectroscopy,[2] tip-enhanced Raman scattering (TERS) spectroscopy,[3] widefield SERS microscopy,[4] SERS holography,[5] time-resolved SERS,[6] or even handheld SERS devices[7]) but also in the design and fabrication of plasmonic substrates.[1c,8]

Porous plasmonic materials offer a versatile platform for significantly enhancing the performance of SERS substrates through multiple synergistic mechanisms. Their high surface-to-volume ratio provides a wealth of active sites for analyte adsorption, directly amplifying the Raman signal.[9] Functioning like a sponge, the porous structure efficiently traps and concentrates analyte molecules within its voids, a feature particularly advantageous for detecting trace analytes in dilute solutions.[10] This localized enrichment increases the likelihood of interaction with the SERS-active surface, enhancing sensitivity for low-abundance molecules in complex matrices such as biological fluids or environmental samples.[11]

A key advantage of metallic porous materials lies in their nanoscale features, such as gaps and crevices between nanoparticles, which generate localized regions of intense electromagnetic fields, known as hot spots.[12] The high density of these hot spots within the porous framework significantly boosts SERS sensitivity. The irregular and interconnected nature of the pores maximizes the number of hot spots, which are critical for achieving strong SERS enhancement.[1b] Moreover, the porous architecture ensures that analyte molecules remain near the SERS-active surface, even for weakly adsorbing species. This proximity stabilizes the SERS signal, improving reproducibility and reliability.[13] The design flexibility of porous materials further extends to their selectivity. By engineering the size, shape, and chemical functionality of the pores, specific molecules can be selectively adsorbed. This is achieved by matching pore dimensions to the analyte or functionalizing pore walls with specific chemical groups. Such tailored porosity enables the detection of target analytes in complex mixtures, minimizing interference from other molecules. This capability is particularly valuable in applications such as drug detection, environmental monitoring, and biosensing.[14] Additionally, the porous structure serves a protective role, shielding SERS-active sites from contamination or degradation. The pores act as barriers to larger molecules or environmental factors, while the ability to remove trapped analytes facilitates substrate regeneration. This enhances the longevity and reusability of SERS substrates, making them more practical for real-world applications.

Porosity in plasmonic materials can be either intrinsic to the metal or introduced through the combination of the plasmonic element with porous coatings or supports, such as porous polymers, mesoporous silica, porous carbon, or metal-organic frameworks (MOFs) as outlined in **Figure 1**. Herein, we will discuss the unique advantages and drawbacks of each of these families of materials for their application in SERS spectroscopy.

M. A. Correa-Duarte
CINBIO
Universidade de Vigo
Vigo 36310, Spain
E-mail: macorrea@uvigo.es
I. B. Becerril-Castro, R. A. Alvarez-Puebla
Department of physical and inorganic chemistry
Universitat Rovira i Virgili
Tarragona 43007, Spain
E-mail: ramon.alvarez@urv.cat
R. A. Alvarez-Puebla
ICREA
Passeig Lluis Companys 23, Barcelona 08010, Spain

DOI: 10.1002/adom.202501376

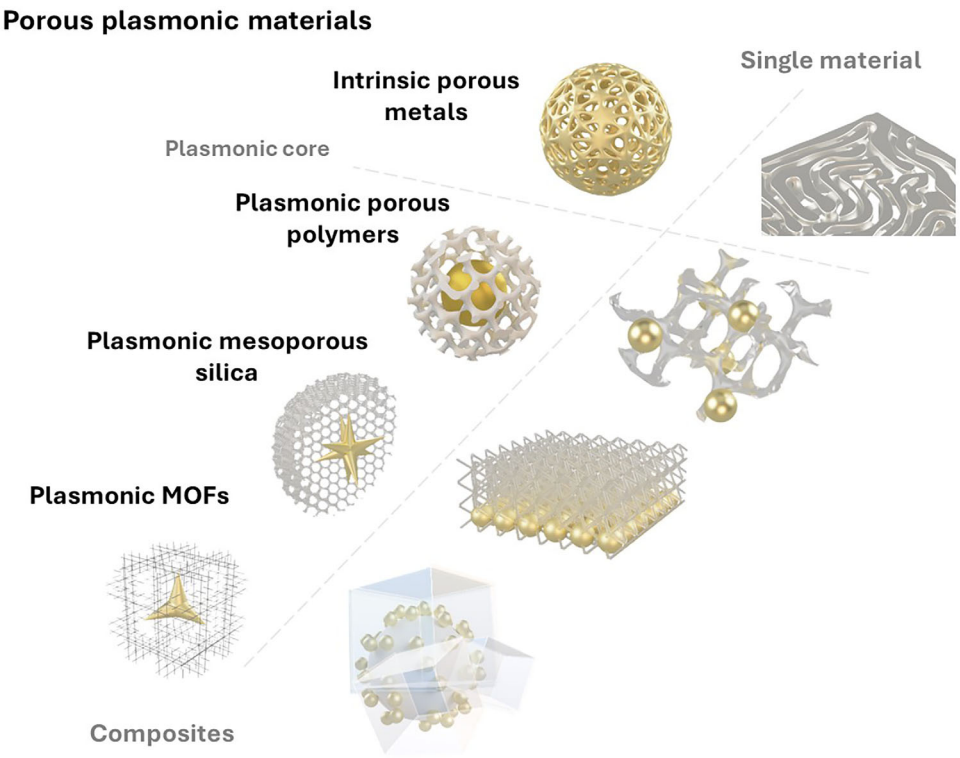

Figure 1. Schematic representation of porous plasmonic materials and their role in SERS enhancement. Intrinsic porous metals exhibit inherent porosity that facilitates strong plasmonic coupling between their nanostructured features, generating a high density of electromagnetic hotspots critical for SERS. These metals can also serve as plasmonic cores within composite architectures, where they are integrated with functional porous matrices to synergistically combine plasmonic activity with tailored material properties. Plasmonic porous polymers offer colloidal stability and stimuli-responsive behavior; mesoporous silica hybrids provide size-selective molecular access, thermal and mechanical resistance and enhanced surface area; and metal-organic frameworks (MOFs) combine extraordinarily precise pore distribution with molecular-level chemical selectivity and targeted analyte enrichment through their crystalline architectures. Together, these composite designs address key challenges in SERS, including stability, selectivity, and controlled molecular trapping near plasmonic surfaces.

2. Intrinsic Porous Metals

Intrinsic porous metals are a class of materials in which porosity is an inherent feature of the metal itself, often achieved through advanced fabrication techniques such as dealloying, templating, or electrochemical deposition. These methods create a network of nanoscale pores and voids within the metal, resulting in a high surface area and abundant plasmonic hot spots.[15] While the synthetic methods to obtain porous metals may vary depending on the format of the plasmonic material (e.g., colloidal nanoparticles or thin films), intrinsic porous plasmonic materials are generally produced using either template-free or templating methods. Template-free methods generate porosity directly from the metal without the use of additional materials such as polymers. Key strategies include dealloying, galvanic replacement, electrochemical degradation, and spontaneous cold welding. Dealloying involves selectively removing one component from an alloy through a corrosion process, where the more electrochemically active elements are dissolved, leaving behind a nanoporous structure composed of the more noble elements. For example, nanoporous gold films are commonly produced by dealloying gold-silver alloys under acidic conditions, where silver is oxidized and dissolved while gold remains metallic (**Figure** 2A).[16] This method has been extended to other alloys, such as AgAl, by selectively dissolving aluminum under appropriate acidic conditions.[17] The initial composition of the alloy allows for some control over the resulting pore sizes. Galvanic replacement is a redox process driven by the difference in reduction potentials between two metals. In this process, one metal is oxidized and dissolved, while the ions of a second metal are reduced and deposited. Popularized by Xia,[18] this method often employs sacrificial nanoparticles of copper, silver, or palladium in contact with solutions containing metal ions with higher reduction potentials such as Au(III) or Pt(II).[19] While galvanic replacement reactions typically preserve the overall morphology of sacrificial colloidal templates, recent advances demonstrate that precisely controlled synthesis conditions can enable the "à la carte" generation of tailored porosity. A representative example of this approach (Figure 2B) begins with well-defined Au octahedra as starting templates, which undergo a sophisticated several transformation process:[19c] i) site-specific Pt deposition preferentially at octahedral edges to create catalytic nucleation sites; ii) controlled etching of interior Au regions to establish an initial porous framework; iii) concentric Au regrowth to reinforce the nanostructure while maintaining porosity; iv) asymmetric Ag deposition to introduce compositional gradients; and v) a final galvanic exchange reaction that produces hollow, highly porous Au octahedral nanosponges (AuOhNSs) with tunable cavity sizes. This

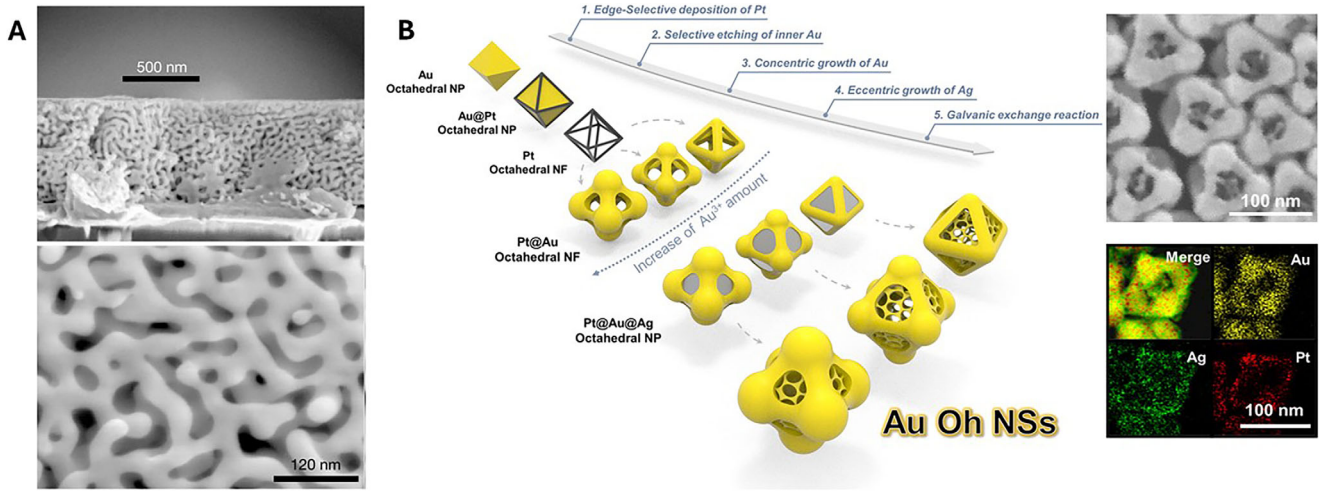

Figure 2. Intrinsic porous metals. A) Cross-section and plan view of a AuAg thin film dealloyed with nitric acid. The porosity is open, and the ligament spacings are of the order of 10 nm. Adapted with permission from ref. [16]. Copyright 2001, Nature. B) Process for the obtention of Au octahedral nanosponges (AuOhNSs). Using Au octahedra as a starting template, multiple chemical steps were applied, including (step 1) edge-selective deposition of Pt, (step 2) selective etching of inner Au, (step 3) concentric growth of Au, (step 4) eccentric growth of Ag, and (step 5) galvanic exchange reaction. Adapted with permission from ref. [19c]. Copyright 2023, American Chemical Society.

multistep methodology illustrates how conventional galvanic replacement can be strategically modified to create complex porous architectures with precisely engineered plasmonic properties for enhanced SERS applications.

The oxidation of silver nanoparticles by gold ions is particularly relevant for SERS. The similar lattice parameters of gold and silver allow them to form solid solutions, but differences in surface tension cause silver to migrate outward while gold moves inward.[20] Since the reduction of one gold atom oxidizes three silver atoms, an excess of gold ions generates nanoporosity throughout the structure while tuning the localized surface plasmon resonances (LSPR).[21] Initially demonstrated in colloidal particles, this process has been adapted to solid thin films, such as by physically evaporating a silver film on a substrate and immersing it in a gold ion solution.[22]

Electrochemical degradation serves as an effective method for inducing controlled porosity in plasmonic nanostructures through redox reactions. This approach has deep historical roots in surface-enhanced Raman spectroscopy (SERS), dating back to the seminal 1974 work of Fleischmann, Hendra, and McQuillan.[23] Their initial observation of enhanced pyridine Raman signals on roughened silver electrodes, originally attributed to increased surface area from oxidation-reduction cycling, laid the foundation for understanding how electrochemical processes can generate nanostructured surfaces. While we now recognize that electromagnetic enhancement from nanoscale features dominates the SERS effect, these electrochemical methods remain valuable for creating nanoporous plasmonic materials. A contemporary example includes the formation of nanoporous gold surfaces through oxidation of carbon monoxide with ozone,[24] where controlled electrochemical cycling produces tunable pore structures ideal for plasmonic applications.

An alternative template-free approach involves spontaneous cold welding of nanoparticles at interfaces. This phenomenon is particularly well-documented for gold nanoparticles functionalized with weakly bound ligands. When these nanoparticles self-assemble at air-water interfaces, they form uniform monoparticulate films that can be transformed into 3D porous architectures through mild thermal treatment or cold welding.[25] The cold welding process preserves nanoscale porosity while creating mechanically robust, interconnected plasmonic networks, making this method particularly attractive for fabricating SERS substrates with both high enhancement factors and structural stability.

Templating methods are highly relevant for fabricating plasmonic materials with intrinsic porosity, as they provide control over structural and morphological features. Templates not only guide microstructure design but also support gelation and maintain structural integrity.[15] Common sacrificial templates include polymer sponges, polystyrene microspheres,[26] dextran,[27] and polyurethane.[28] After depositing plasmonic metals (e.g., gold or silver) or mixing their precursors with the template, the template is removed through solvent dissolution or calcination, leaving behind a porous metal framework. However, high-temperature processes often result in larger feature sizes and reduced specific surface areas, which can limit plasmonic performance. An alternative approach involves ice templating, where freezing and drying concentrated nanoparticle solutions produce monolithic foams with intrinsic porosity.[27,29] This method relies on freezing-induced phase separation, nanoparticle accumulation, and ice sublimation to form porous networks.[30] While effective for creating lightweight, porous plasmonic materials, ice templating requires high precursor concentrations and often yields materials with lower specific surface areas.

The unique nanoscale roughness and interconnected pore networks of intrinsic porous metals generate a high density of electromagnetic hotspots, which are essential for achieving strong SERS signals.[19c] As demonstrated in **Figure 3**A, optical simulations of surface charge and near-field distributions reveal significant charge localization and dramatically enhanced near-field intensities at the tips of porous metal structures (right panels) compared to their non-porous counterparts. These

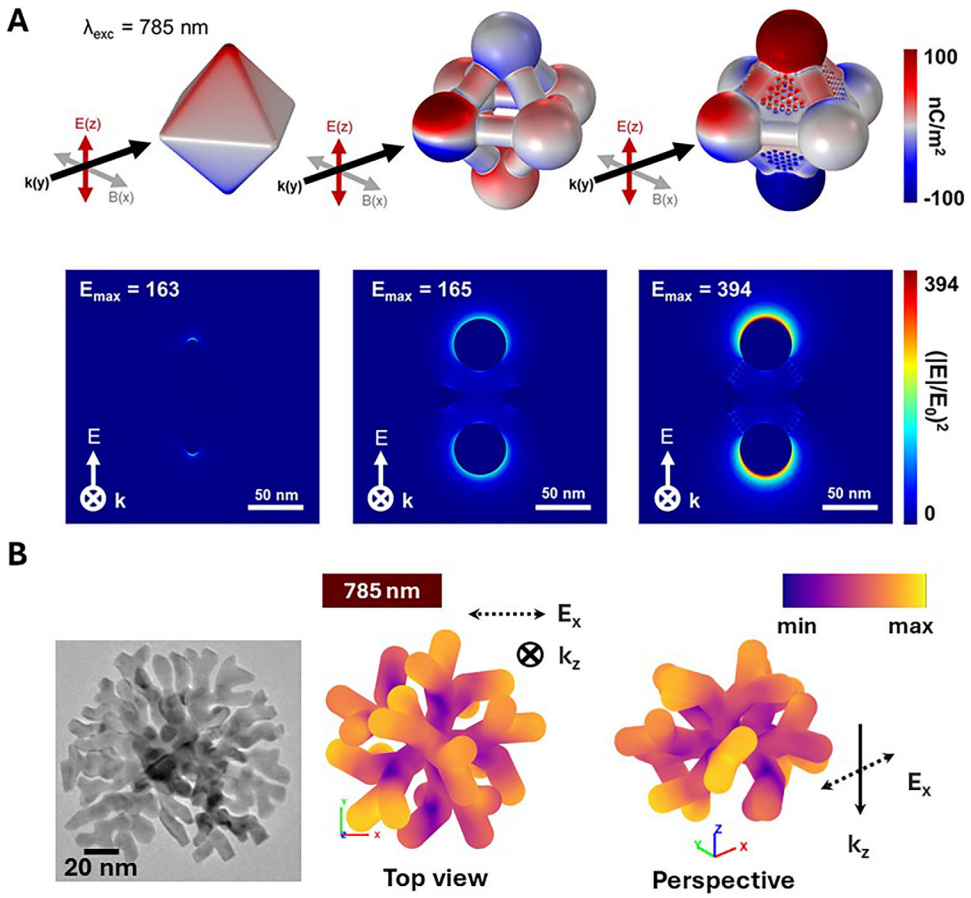

Figure 3. Plasmonic distributions in intrinsic porous metals. A) Surface charge distributions (top) and near-field enhancements (bottom) at 785 nm excitation comparing three gold morphologies: solid octahedra (left), tip-modified octahedra (center), and porous octahedra (right), demonstrating enhanced electromagnetic fields in porous structures. Scale bars: 50 nm. Adapted with permission from ref. [19c]. Copyright 2023, American Chemical Society. B) High-resolution TEM revealing nanoscale porosity in gold architectures (adapted with permission from ref. [28]. Copyright 2010, American Chemical Society) and boundary element method (BEM) simulations of structure under 785 nm excitation, showing localized field enhancements at interparticle junctions.

simulations clearly illustrate how the porous architecture facilitates plasmonic coupling, with experimental studies showing that intrinsic porous metals consistently achieve SERS enhancement factors at least two orders of magnitude greater than solid nanostructures.[31] When the size of the branches increase, such in the case of gold lace nanoshells,[28] the intricate porous morphology creates a complex network of plasmonically active branches and gaps. The boundary element method (BEM) simulations (Figure 3B) of these nanostructures under 785 nm excitation, clearly shows the intense electric field enhancements (hotspots) concentrated at the interbranch junctions. This remarkable field confinement, combined with the structural reproducibility of these materials, enables highly sensitive single-particle SERS spectroscopy,[28] making them exceptional substrates for molecular detection applications.

Plasmonic metals including gold, silver, and copper have emerged as particularly advantageous for constructing porous SERS substrates due to their unique combination of intrinsic optical properties, chemical stability, and structural robustness. Gold stands out for its exceptional resistance to oxidation and corrosion, maintaining its plasmonic performance even under harsh environmental conditions or prolonged laser exposure. Silver, while slightly more chemically reactive, exhibits superior plasmonic activity in the visible spectrum due to its strong optical response and lower optical losses compared to other metals. Copper represents a more economical alternative that, despite its greater susceptibility to oxidation, demonstrates satisfactory plasmonic behavior when properly protected, making it viable for cost-sensitive applications. These inherent material properties collectively enable the development of intrinsic porous metal substrates capable of withstanding demanding SERS measurement conditions, including high laser power densities and aggressive chemical environments, while maintaining long-term signal stability and reproducibility.

A key advantage of intrinsic porous metals lies in their self-contained plasmonic functionality. These monolithic metallic structures generate electromagnetic hotspots through their inherent nanoscale porosity. Practical implementations of these SERS substrates have demonstrated exceptional capabilities for noninvasive disease diagnosis (**Figure** 4A).[31] The Au@Ag-Au porous nanoframes (PNFs), functionalized with cysteine (Cys, Figure 4Aa), enables selective detection of benzaldehyde (BA)

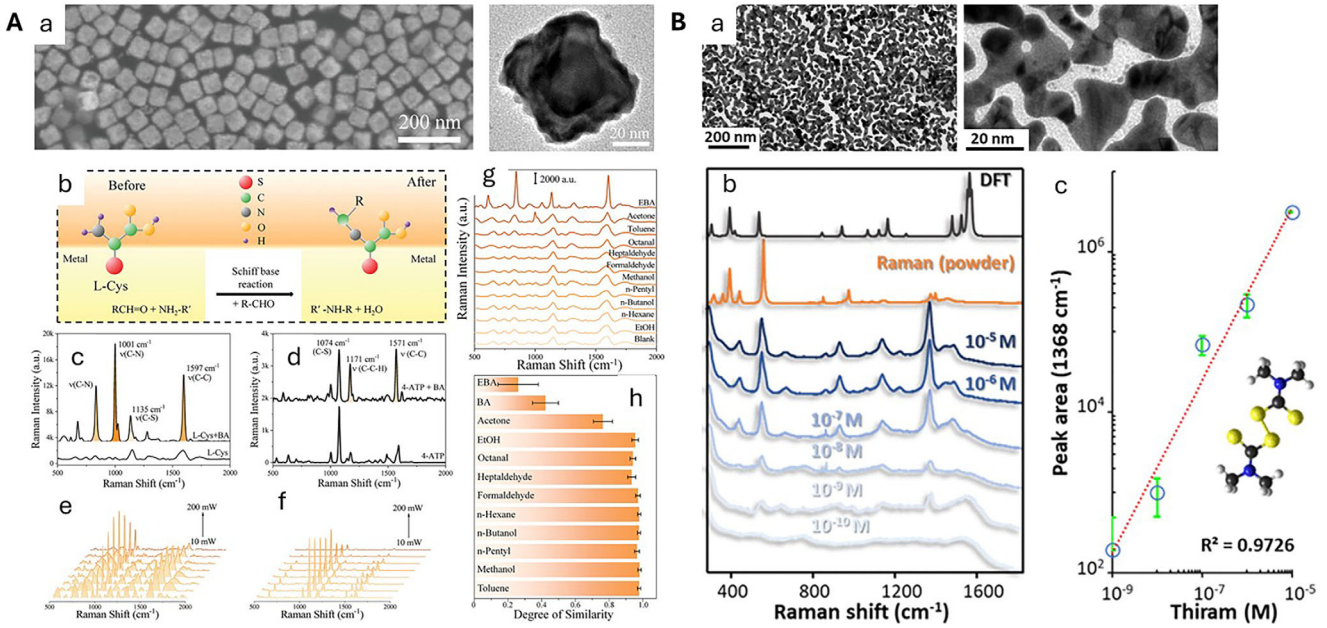

Figure 4. Performance evaluation of porous metal SERS substrates under challenging conditions. A) Use of porous nanoframes (PNFs) for the evaluation of lung cancer markers in breath exhalates. a) Structural overview of galvanically displaced PNFs; b) Reaction scheme between cysteine (Cys) and benzaldehyde (BA); c,d) SERS spectra tracking molecular modifications on Cys- and aminothiophenol (ATP) functionalized surfaces; e,f) Power-dependent stability assessment; g,h) Specificity analysis against potential interferents. Adapted with permission from ref. [31]. Copyright 2025, Wiley VCH. B) Thiram detection in waters using gold porous films: a) Cold-welded film morphology; b) SERS spectra of thiram in water, contaminated with different concentrations of the analyte, on the porous cold-welded film; c) correlation of the peak area of the CS stretching with the thiram concentration. Adapted with permission from ref. [25]. Copyright 2019, Wiley VCH.

and related aldehydes in exhaled air—key biomarkers elevated in cancer patients (Figure 4Ab). The substrate's 3D porous architecture facilitates efficient gas transport, while the L-Cys modification specifically captures BA via Schiff base reactions, evidenced by characteristic C=N peaks at 835 and 1001 cm^{-1} (Figure 4Ac). Comparative studies with aminothiophenol (ATP) modified substrates revealed superior stability of Cys under laser irradiation (Figure 4Ae,f), with minimal interference from other volatile organic compounds (Figure 4Ag,h). Similarly, cold-welded porous gold films overcome intrinsic limitations for detecting thiram, a pesticide with an inherently small SERS cross-section (Figure 4B),.[25] Unlike conventional substrates that sample microliter volumes, these films first adsorb and concentrate thiram molecules onto nanoparticles, which then migrate to form a porous interfacial layer (Figure 4Ba), amplifying local analyte concentrations by orders of magnitude. The cold-welding process creates homogeneous hotspots across the entire surface, eliminating signal variability seen in randomly assembled cast/evaporated films. The linear correlation between CS stretching intensity (1369 cm^{-1}) and thiram concentration enables ultrasensitive quantification (Figure 4Bb,c).

Despite their advantages, intrinsic porous metals have several limitations. First, while their plasmonic properties are excellent, controlling pore size and distribution with high precision remains a significant challenge. Variations in pore geometry can lead to inconsistent electromagnetic field enhancement, limiting their selectivity for specific analytes, particularly in complex mixtures. Second, because the entire material is optically active, the porosity cannot be exploited as a size-selective barrier to filter or sieve analytes based on molecular dimensions. Finally, the reliance on precious metals such as gold and silver can be cost-prohibitive for large-scale applications. Additionally, the fabrication processes for these materials—such as dealloying, templating, or electrochemical deposition—are often time-consuming and resource-intensive, further limiting their scalability.

3. Plasmonic Porous Polymers

Plasmonic porous polymers combine polymer matrices with plasmonic nanoparticles to significantly enhance Raman signal intensity for adsorbed analytes. The porous polymer matrix provides a high surface area, increasing adsorption sites for target molecules and improving sensitivity.[32] These polymers can be tailored to selectively adsorb molecules based on size, polarity, or chemical affinity, enhancing SERS specificity and reducing interference from non-target substances.[33] Additionally, embedding nanoparticles within the polymer matrix prevents aggregation and oxidation, ensuring substrate stability and prolonged functionality.[34] The polymer also imparts mechanical robustness, facilitating applications in laboratory, field, or clinical settings.

These materials typically adopt two structural configurations: single nanoparticles coated with a porous polymer shell and polymer frameworks embedding plasmonic nanoparticles within their porous structures. In the first configuration, a porous polymer layer encapsulates individual nanoparticles, preserving their plasmonic properties while providing a protective, functional coating. The synthesis involves nanoparticle

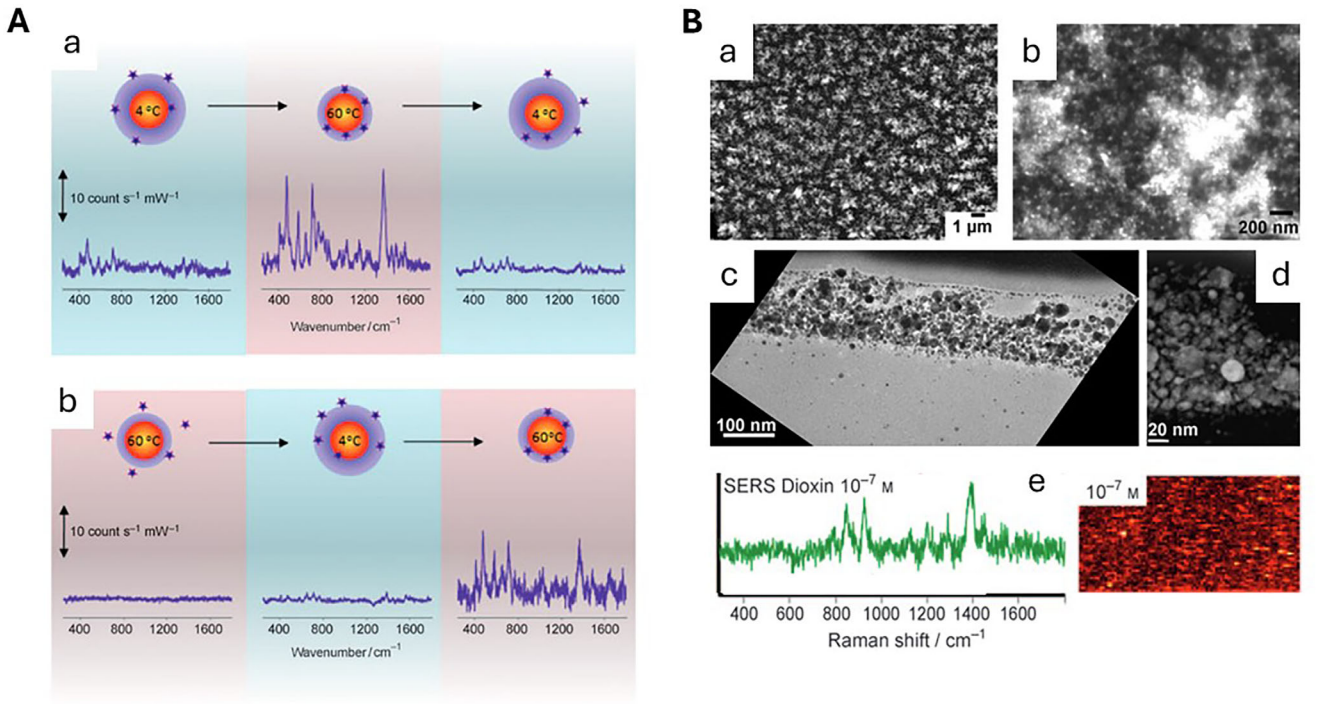

Figure 5. Plasmonic porous polymers. A) SERS spectra of 1-naphthol on Au@pNIPAM core–shell particles, as a function of the solution temperature in two different cooling-heating cycles: a) from 4 to 60 to 4 °C; and, b) from 60 to 4 to 60 °C. Excitation line 780 nm, acquisition time 2 s. Reproduced with permission from ref. [38]. Copyright 2009, Wiley VCH. B) Top-view SEM images a,b) at different magnifications of the e-LBL AgNP film after 24 h of immersion. Cross-sectional TEM and STEM images c,d) of the film after focused ion beam (FIB) preparation. e) SERS spectrum and imaging of a dioxin on the film, measured with a 633 nm laser line. Reproduced with permission from ref. [45]. Copyright 2009, Wiley VCH.

formation, functionalization with polymerization initiators, and in situ polymerization. The plasmonic core can be tailored to various morphologies—such as spheres, cubes, rods, or stars—depending on the application. For instance, spherical nanoparticles, which require high particle densities for SERS signals, are commonly used in colloidal form for average SERS.[35] In contrast, nanostars[35] or single-particle aggregates[36] can deliver single-particle SERS signals and are often employed in isolated or patterned films.[37] Polymer coatings may include functional materials like poly(N-isopropylacrylamide) (PNIPAM),[32b,38] polymethacrylic acid (PMAA)-polyethylene glycol (PEG),[39] or poly(styrene-alt-maleic acid).[40]

Gold nanoparticles coated with poly(N-isopropylacrylamide) (PNIPAM) exhibit temperature-responsive behavior due to the polymer's reversible phase transition near its lower critical solution temperature (LCST, ≈32 °C).[41] Below the LCST, the hydrophilic, swollen PNIPAM keeps the nanoparticles dispersed, yielding weaker SERS signals. Above the LCST, hydrophobic collapse brings nanoparticles closer, increasing local analyte concentration and enhancing SERS intensity. These systems can be implemented as single-coated nanospheres measured in colloidal suspension or as single-particle hot-spot configurations using nanostars as plasmonic cores. **Figure** 5A demonstrates this thermoresponsive concept with gold nanospheres in two different temperature cycles. Alternatively, solid thin films can be fabricated by coating continuous plasmonic substrates with PNIPAM[42] or organizing PNIPAM-coated particles into patterned surfaces.[37] Similar stimuli-responsive effects are achievable with pH-sensitive systems, such as PMAA-PEG hybrids.[39]

Beyond conventional designs, nanoparticle-polymer composites can be precisely engineered through layer-by-layer (LbL) assembly to create hierarchically structured platforms with alternating plasmonic and polymer strata. These sophisticated multilayered architectures offer tunable molecular selectivity through three key mechanisms: i) size-exclusion via controlled interlayer spacing, ii) polarity-dependent partitioning through tailored polymer chemistries, and iii) specific chemical interactions with functionalized interfaces.[43] For enhanced plasmonic performance, exponential LbL (e-LbL) growth techniques[44] enable precise control over the density and spatial distribution of plasmonic elements within the polymer matrix. A demonstration of this approach is shown in Figure 5B, where infiltration of e-LbL films with silver nanoparticles (AgNPs) creates a percolating 3D network of electromagnetic hot spots.[45] This design achieves exceptional SERS enhancement factors (exceeding10^8) across a broad spectral range (400–1200 nm), making it particularly valuable for near infrared-SERS applications where reduced background interference and deeper tissue penetration are critical. Incorporating plasmonic nanoparticles into polymeric matrices produces advanced SERS substrates that merge the optical properties of metals with the structural advantages of 3D networks. These hybrid materials outperform rigid substrates in sensitive molecular detection, particularly for biomedical and environmental applications,[46] due to the synergy between electromagnetic enhancement and molecular sieving.

Two primary synthetic approaches dominate: in-situ nanoparticle formation and post-synthetic infusion. Hydrogels embed pre-formed nanoparticles during polymer cross-linking, ensuring uniform distribution for biomolecular interactions.[47] Aerogels employ sol-gel chemistry with metal precursors before supercritical drying, allowing precise control over nanoparticle size and distribution.[15b,48] Recent advances include photo-patterning for spatially controlled hotspots and microwave-assisted synthesis for rapid nanoparticle deposition.[49]

Hydrogels excel in aqueous-phase detection due to their hydrated, porous structure. Tunable mesh sizes selectively concentrate analytes near plasmonic hotspots while maintaining biocompatibility.[50] Gold nanoparticle-enriched poly(acrylamide-co-acrylic acid) hydrogels achieve clinically relevant detection limits for cancer biomarkers with rapid response times,[51] making them suitable for wearable diagnostics and microfluidic systems. Bulk hydrogel-based nanocomposites demonstrate exceptional potential as molecular concentrators for ultratrace SERS detection, as exemplified by silver nanoparticle-loaded agarose systems. These porous architectures function as mechanically responsive traps that reversibly concentrate analytes through gel collapse upon drying, a process that simultaneously enhances SERS sensitivity by forcing plasmonic nanoparticles into closer proximity, thereby generating dynamic electromagnetic hotspots. The hydrogel's rehydration capability enables remarkable recyclability, as embedded silver nanoparticles remain physically constrained within the polymer network while analytes can be completely removed through simple dialysis. This unique combination of properties was successfully employed for the first reported SERS detection of dichlorodiphenyl-trichloroethane (DDT), overcoming the traditional challenges associated with this non-ideal SERS analyte. The system's reversible sequestration capability, coupled with its tunable hotspot generation mechanism, establishes aerogel composites as a promising platform for environmentally persistent pollutant monitoring with potential for multiple reuse cycles.[10]

Conversely, aerogels are ideal for gas-phase sensing due to their exceptional porosity (>90%) and ultralow density (<0.1 g cm^3).[52] Silver-functionalized aerogels detect volatile organic compounds at picomolar levels, offering superior environmental monitoring capabilities.[49b] Their robust yet porous framework prevents nanoparticle aggregation, ensuring long-term stability.[53] Gas monitoring can be also achieved using a plasmonic aerogels. For example acrylamide/bis-acrylamide polymerization in gold nanocube solutions, followed by freeze-drying to create a macroporous (≈100 µm) 3D scaffold with a surface area of160 m^2 g with embedded nanoparticles. This lightweight architecture demonstrates exceptional SERS enhancement, enabling sensitive optical detection when functionalized with iron porphyrin to create a reversible CO sensor. The system shows linear response across the critical 10–40 ppm concentration range, covering health-relevant thresholds, with rapid 30-second recovery, making it particularly suitable for real-time environmental monitoring applications.[54]

Plasmonic particle-polymer composites offer high sensitivity, enhanced Raman signals, design flexibility, and cost-effective scalability. Applications span environmental sensing, biomedical diagnostics, food safety or catalytic monitoring. However, challenges remain, including stability under harsh conditions, nanoparticle uniformity, batch-to-batch reproducibility, and limited optical access in densely loaded structures.

4. Plasmonic Mesoporous Silica

Mesoporous silica-coated plasmonic nanoparticles combine the strong electromagnetic field enhancement properties of plasmonic metal cores (typically gold or silver) with the high surface area, tunable porosity, and robust surface chemistry of mesoporous silica shells. Unlike conventional dense silica coatings, mesoporous silica can contain an ordered network of nanopores (typically 2–6 nm in diameter),[55] arranged in a uniform, sponge-like matrix with surface areas ranging from 300 to 1000 m^2/g. This unique architecture enables not only enhanced plasmonic signal amplification but also the adsorption, storage, and controlled release of small molecules—making these particles ideal for SERS, drug delivery, catalysis, and biosensing.

The synthesis of these nanoparticles typically involves a multistep process to ensure uniform coating and controlled pore formation. First, plasmonic metal cores are synthesized via chemical reduction methods and then functionalized with a stabilizing agent, such as cetyltrimethylammonium bromide (CTAB) or (3-aminopropyl)triethoxysilane (APTES), to promote adhesion of the silica shell.[56] A thin, dense silica layer is often deposited first to prevent metal-mesopore interactions and ensure uniform growth of the subsequent mesoporous shell. The mesoporous silica coating is then formed via a sol-gel process using tetraethyl orthosilicate (TEOS) as the silica precursor and CTAB as a structure-directing agent. The CTAB micelles act as templates for pore formation, and their removal via calcination (400 °C, 4 h) or solvent extraction (e.g., acidic ethanol reflux) leaves behind an open, accessible pore network. By carefully adjusting reaction parameters such as surfactant concentration, TEOS addition rate, and reaction time, the pore size, shell thickness, and overall particle morphology can be tuned for specific applications.

Mesoporous silica-coated particles can consist of single particles of any morphology, including nanospheres, nanorods and nanotriangles (**Figure 6A**).[56] Although these were the first to be prepared, they suffer from several limitations. First, only specific particle shapes can sustain electromagnetic fields strong enough to provide sufficient SERS enhancements for detection, and the silica coating often passivates part of the plasmonic surface. As a result, such particles are primarily used for encoding applications,[59] such as labeling micro-objects (e.g., cells),[60] or macro-objects (e.g., anti-counterfeiting tags).[61] An alternative to overcome these drawbacks is the use of yolk-shell structures with efficient plasmonic cores, such as nanostars in Figure 6B.[57] This configuration allows for greater analyte loading while the nanostar acts as a single-particle hot spot. However, these particles remain below the Rayleigh diffraction limit and thus cannot be observed under conventional optical microscopes used in micro-Raman systems. Notably, submicro- and micro-objects, such as polystyrene beads, can be coated with plasmonic nanoparticles[62] and subsequently encapsulated in mesoporous silica. The polymeric core can then be removed via dissolution or calcination,[63] yielding a hollow porous capsule with an inner plasmonic layer or a network of interacting nanoparticles (Figure 6C). This architecture provides selective permeability: small analyte molecules

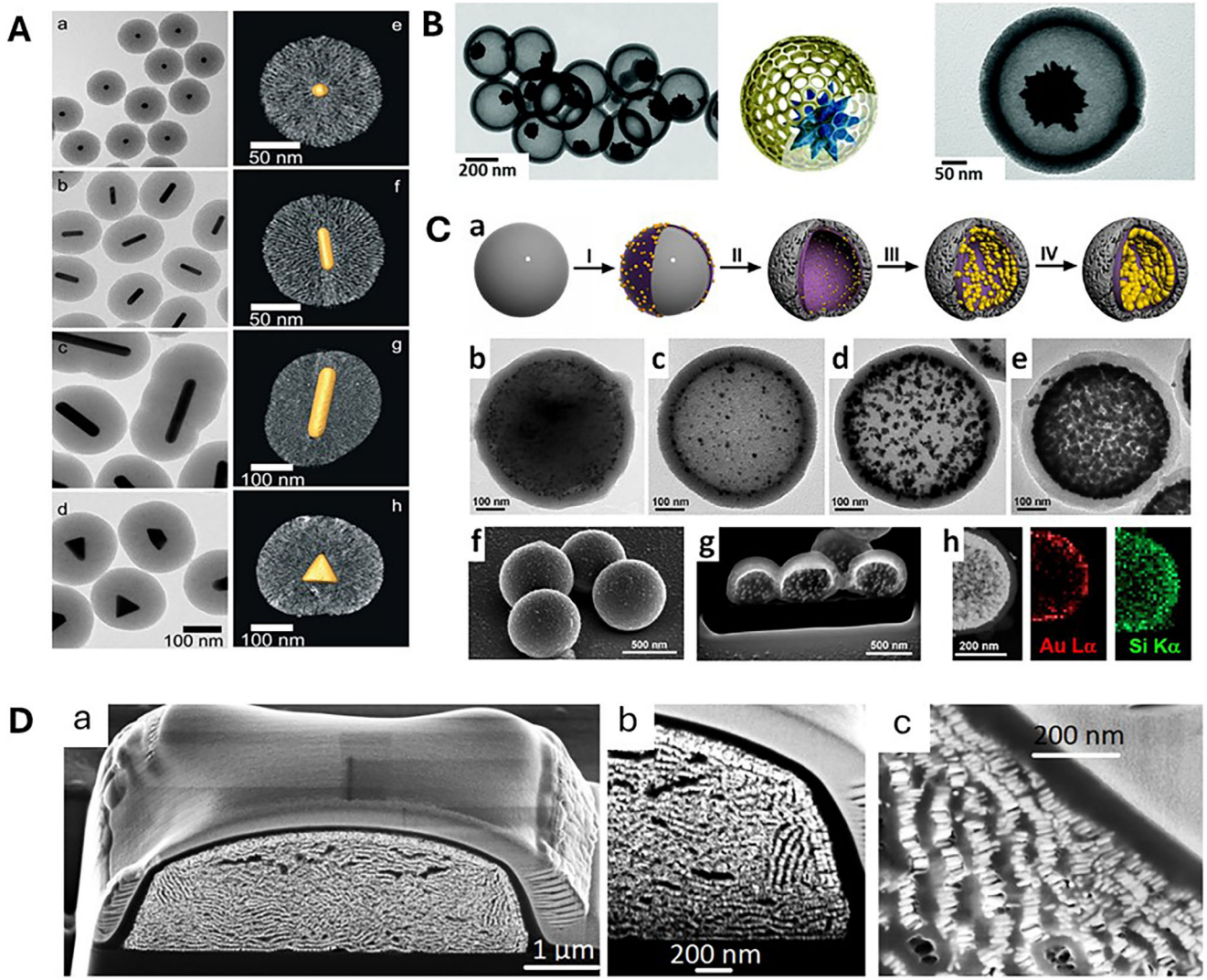

Figure 6. Plasmonic porous silica. A) 2D and 3D TEM characterization of hybrid nanostructures containing gold nanoparticles with various shapes: nanospheres a,e), single-crystal nanorods b,f), pentatwinned nanorods c,g), and nanotriangles d,h). Reproduced with permission from ref. [56]. Copyright 2015, American Chemical Society. B) Yolk-shell gold nanostars coated with mesoporous silica. Reproduced with permission from ref. [57]. Copyright 2019, Royal Society of Chemistry. C) a) Fabrication of plasmonic hollow capsules (gold deposition on polystyrene beads, mesoporous silica coating and polystyrene calcination, and gold overgrowth); b–e) TEM images of the fabrication process; f,g) SEM-FIB characterization; and, EDAX chemical analysis of the capsules. Reproduced with permission from ref. [55]. Copyright 2019, Wiley VCH. D) Mesoporous silica coating of gold nanorod supercrystals. Reproduced with permission from ref. [58]. Copyright 2016, Nature Publishing Group.

diffuse through the pores to interact with the metal surface or embedded chemosensors, while larger biomolecules, cells, or contaminants are excluded (**Figure** 7A). Such molecular sieving is particularly advantageous in complex biological or environmental samples, where interfering species could otherwise quench the signal or foul the nanoparticle surface.[55] The plasmonic layer generates a dense array of hot spots (Figure 7B),[63a] reminiscent of plasmonic island films,[64] which can be further overgrown if desired.[63b] Notably, LSPR excitation inherently produces heat.[65] In plasmonic hollow shells, this heat is confined within the silica capsule, leading to a localized temperature increase inside the cavity while leaving the external environment unaffected (Figure 7C).[63a] This internal heating also induces convective flow, enhancing the exchange of small molecules between the capsule's interior and exterior. Thanks to these properties, plasmonic hollow capsules have been employed as nanoreactors for thermally controlled Diels-Alder reactions, with operando SERS monitoring reaction kinetics (Figure 7D),[63a] and as intracellular sensors for real-time tracking of nitric oxide production in living organisms (Figure 7E).[66]

Finally, plasmonic films can be also coated with mesoporous silica (Figure 6D).[58,67] In such a cases, the final goal, as in the previous materials, is to create selective permeability: where small analyte molecules diffuse through the pores to interact with the metal surface or while larger biomolecules, cells, or contaminants are excluded. Applicability of these materials had been demonstrated in the SERS quorum sensing of the growth of bacteria colonies, where the molecules responsible of such

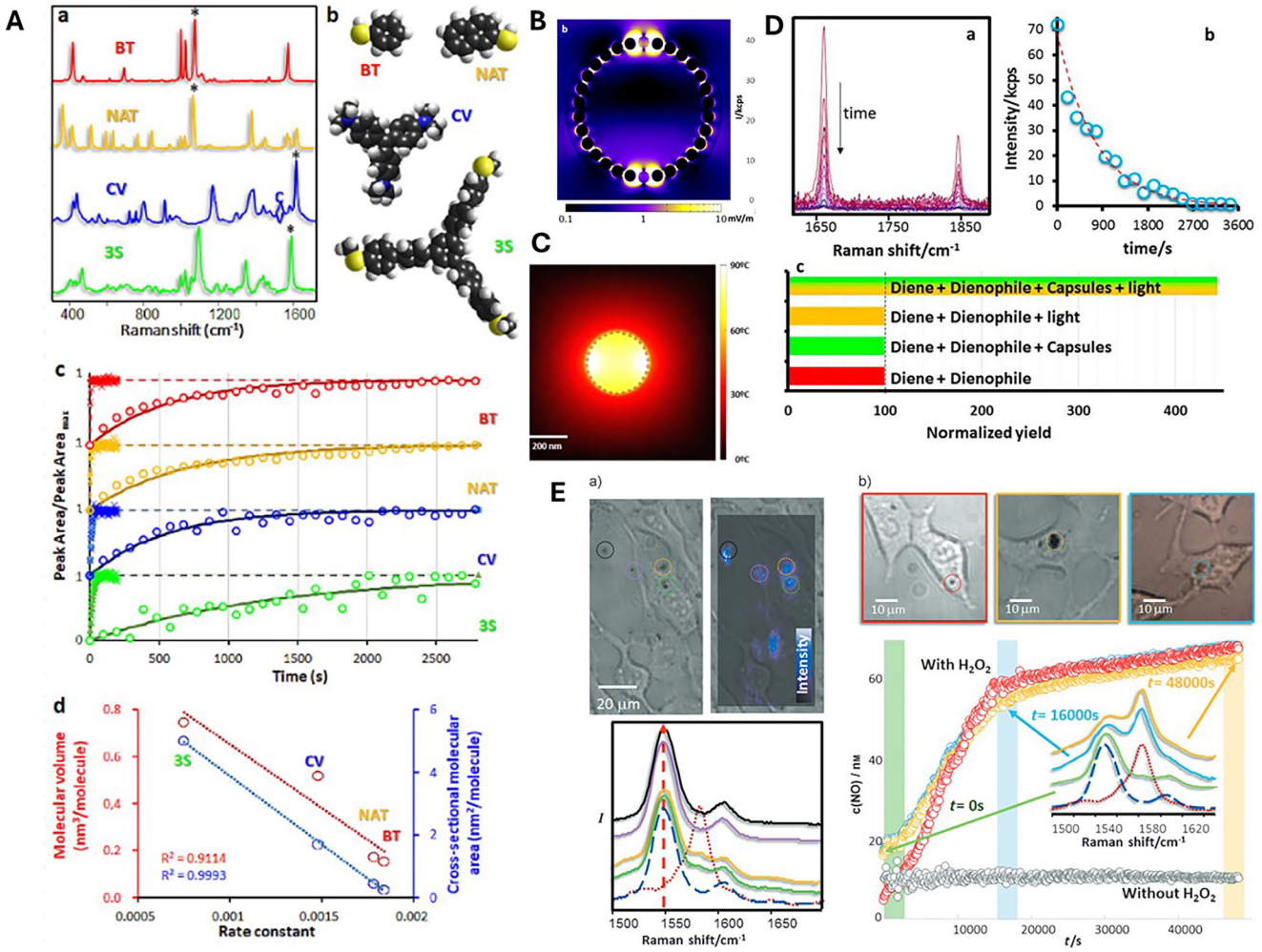

Figure 7. A) a) SERS spectra and b) molecular structure of SERS probes with differnt molecular volumes used for the exploration of the porous structure of the capsules. c) Sorption kinetics of the different probes onto the inner gold films of the capsules (circles and solid lines) or onto bare PS@Au beads (crosses and dotted lines). d) Comparison of the sorption rate constant of the different probes on the capsules with their molecular volume ad their molecular cross-sectional area. Reproduced with permission from ref. [55]. Copyright 2019, Wiley VCH. B,C) Theoretical calculations of near electromagnetic field and the temperature of a plasmonic hollow capsule upon excitation with 785 nm laser line. D) a,b) SERS monitoring of a Diels-Adler reaction occurring inside the nanocapsule over the time. c) Comparison of the reaction yields after 30 min determined by ^{1}H NMR for our system and controls including the diene and dienophile in the presence and absence of capsules and light. Reproduced with permission from ref. [63a]. Copyright 2013, American Chemical Society. E) a) Optical and SERS (mapped at 1548 cm^{-1}, as marked below) images of 3T3 cells in the presence of plasmonic hollow capsules. The SERS spectra (bottom) show the signals for the colored circles in the image (top). b) Optical images and intracellular nitric oxide (NO) formation over time (obtained through the I1583/(I1583+I1548) relation) for three different samples upon NO induction with oxygen peroxide (H_2O_2). A control sample without the presence of H_2O_2 is also shown for comparison. Representative normalized SERS spectra obtained at different times are shown. Reproduced with permission from ref. [66]. Copyright 2013, Wiley VCH.

quorum sensing have low SERS cross/section and thus requires of highly efficient plasmonic materials to be detected,[58] or in the operando SERS monitoring of the atmospheric nitrogen reduction to ammonia photocatalysis.[68]

5. Plasmonic Metal-Organic Frameworks

MOFs represent a class of highly ordered; porous crystalline materials formed through the coordination of metal ions with organic linkers. These hybrid materials combine exceptional porosity with remarkable structural diversity, offering surface areas that can exceed 5000 m^2 g – far surpassing traditional porous materials like mesoporous silica (≈1000 m^2 g) or polymeric frameworks. This unique combination of properties has positioned MOFs as ideal candidates for SERS applications, where they serve to both amplify and refine the detection capabilities of plasmonic nanostructures.[69] The fundamental advantage of MOFs in SERS applications lies in their precisely tunable architecture. Unlike mesoporous silica with its fixed pore size distribution (typically 2–50 nm), MOFs enable exact control over pore dimensions – from micropores (<2 nm) to mesopores (2–50 nm) – through careful selection of metal nodes and organic linkers. This tunability permits size- and shape-selective molecular recognition, allowing for the selective enrichment of target analytes while ex-

cluding potential interferents from the plasmonic hotspots.[69–70] Moreover, the chemical environment within MOF pores can be precisely engineered through functional group modification of the organic linkers, enabling tailored interactions with specific analyte classes.

The integration of MOFs with plasmonic nanoparticles has led to the development of several hybrid architectures, each designed to optimize SERS performance. Core-shell configurations, where plasmonic nanoparticles are completely encapsulated within a MOF matrix, represent the most common design.[71] In these structures, the MOF shell serves multiple functions: it physically protects the metal core from oxidation and aggregation, provides selective molecular access to the plasmonic surface, and can participate in charge-transfer processes that complement the electromagnetic enhancement mechanism. The high porosity of MOFs ensures rapid analyte diffusion to the active sites while maintaining structural stability.[72] To address the challenge of achieving sufficient electromagnetic field enhancement, nanostar-core structures can be used to generate intense local fields at sharp metallic tips,[73] yolk-shell designs incorporating bilayered MOFs for controlled release and detection,[74] and plasmonic arrays assembled on polymer bead templates that provide high-density hot spots.[13,75]

The fabrication of MOF-coated plasmonic nanoparticles employs several established methods, each offering distinct advantages depending on the desired application. The direct growth method is a one-pot approach involving simultaneous presence of plasmonic nanoparticles and MOF precursors in solution under carefully controlled conditions. For instance, ZIF-8 coatings can be grown on gold nanoparticles by combining $HAuCl_4$, Zn^{2+} ions, and 2-methylimidazole in methanol. This method allows for straightforward scalability; however, its effectiveness requires precise optimization of temperature, pH, and solvent composition.[76] Layer-by-layer assembly initiates with functionalization of plasmonic particles using charged polymers or specific ligands that enhance MOF precursor adhesion, enabling nanometer-scale control over coating thickness as demonstrated in MOF-199 (HKUST-1) shells on silver nanocubes.[77] Seed-mediated growth attaches pre-synthesized MOF nanocrystals to plasmonic particles through electrostatic interactions or covalent bonding before further growth, producing uniform coatings as seen in UiO-66-NH_2 shells on gold nanorods.[76,78] The template sacrifice method creates hollow MOF shells encapsulating plasmonic cores through sacrificial layer removal, exemplified by Au@ZIF-8 yolk-shell structures where silica templates are dissolved using sodium hydroxide.[79] While architecturally sophisticated, this multi-step technique poses scaling challenges.

Recent advances have demonstrated the successful integration of plasmonic MOFs into SERS-based detection systems. A notable example includes MOF-functionalized silver nanoparticles that achieved ultra-sensitive pesticide analysis in agricultural samples.[80] Similarly, innovative 3D MOF architectures have shown exceptional potential for continuous atmospheric monitoring of CO_2, highlighting their environmental sensing capabilities even remotely (**Figure 8A**).[81] Recent advances in stand-off SERS spectroscopy now enable real-time, multiplex detection of airborne species by integrating long-range optics with Ag@MOF core–shell nanoparticle assemblies. These 3D plasmonic architectures create micrometer-thick SERS hotspots that actively sorb and detect aerosols, gases, and VOCs at parts-per-billion concentrations across distances up to 10 m. The platform demonstrates remarkable sensitivity to atmospheric changes, as evidenced by cyclic CO_2; monitoring and outdoor quantification of polycyclic aromatic hydrocarbons under daylight interference. By combining micron-scale analyte capture with remote Raman detection (2-10 m range), this technology overcomes traditional limitations in stand-off spectroscopy, establishing new paradigms for environmental monitoring, disaster prevention, and security applications where molecular-level air surveillance is critical.

The engineered hydrophobicity of MOFs plays a pivotal role in SERS enhancement. By strategically modifying MOF structures, for instance, through hydrophobic ligand incorporation, these materials can effectively concentrate non-polar analytes near plasmonic hotspots.[69,82] This molecular trapping mechanism significantly boosts detection sensitivity for typically SERS-inactive hydrophobic compounds.[69] An emerging paradigm in transition metal sensing utilizes MOF-tethered ion-selective dyes as indirect SERS reporters.[83] This approach capitalizes on MOFs' molecular recognition properties to selectively capture target ions, thereby amplifying plasmonic coupling and Raman signal generation.[13] The convergence of MOFs and plasmonics has spawned multifunctional hybrid platforms. One breakthrough application combines hydrophobic MOFs with photothermally active gold nanostars, enabling concurrent drug delivery and SERS-based release monitoring under single-wavelength excitation.[73] Synergistic material combinations further expand SERS functionality. Integrating MOFs with complementary nanomaterials like conductive carbons or catalytic metal oxides creates systems with enhanced sensing performance and additional capabilities.[72,84] Particularly noteworthy are operando configurations where plasmonic excitation simultaneously drives photocatalytic reactions and enables real-time mechanistic studies through SERS monitoring (Figure 8B).[75]

6. Conclusions and Outlook

The integration of porous architectures into SERS substrates has revolutionized the field by simultaneously addressing two fundamental challenges: analyte concentration and electromagnetic field enhancement. As demonstrated throughout this review, the strategic design of porosity, whether in intrinsic nanoporous metals, functional polymer matrices, mesostructured silica hybrids, or crystalline MOFs, enables unprecedented control over molecular enrichment and plasmonic coupling. These materials leverage their unique structural features to create synergistic platforms that significantly outperform conventional SERS substrates in sensitivity, selectivity, and reproducibility. However, to fully realize their potential and transition from laboratory prototypes to real-world applications, several critical challenges must be addressed through focused research efforts.

Looking ahead, the field must prioritize the development of porous substrates with precisely engineered architectures. Future work should explore advanced fabrication techniques capable of producing pores with atomic-scale uniformity, such as MOF-templated growth or optimized dealloying protocols, to ensure reproducible hotspot generation. The creation of gradient porous structures, combining meso- and macroporous domains, could optimize the balance between molecular diffusion

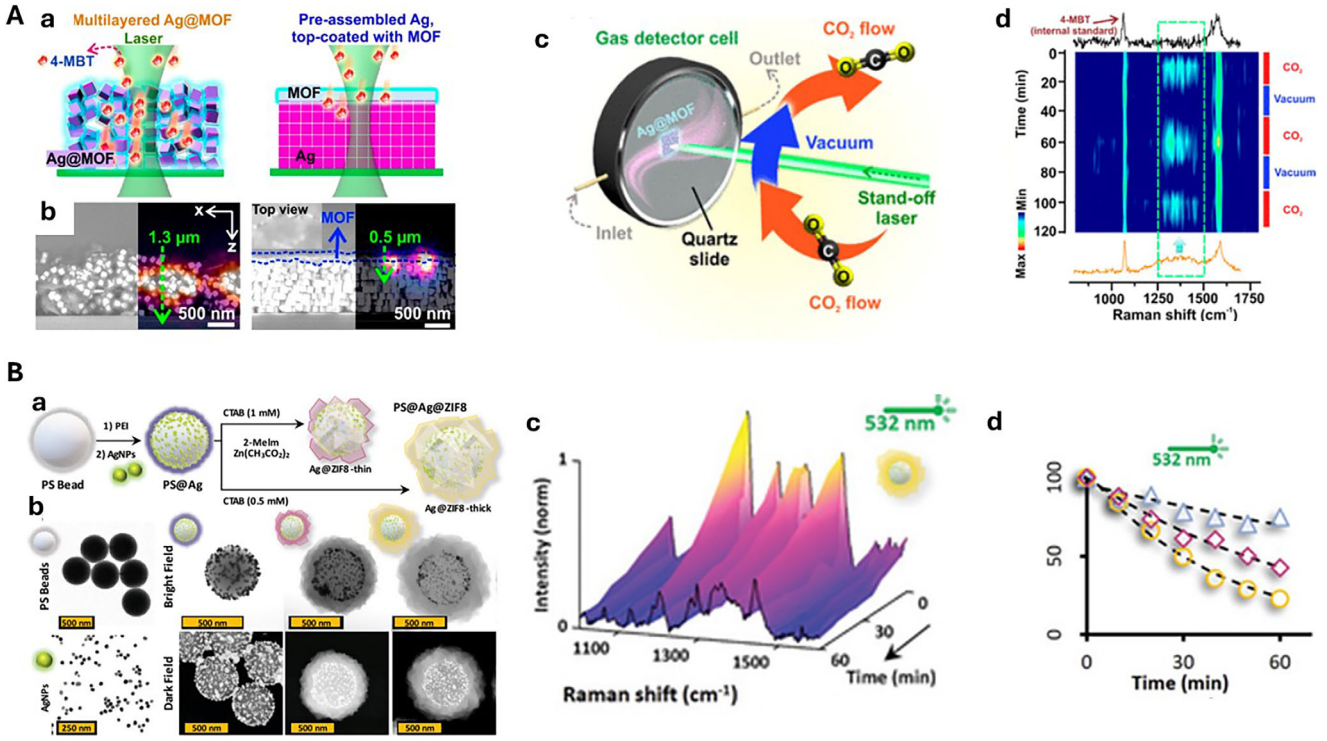

Figure 8. A) Remote MOF-SERS platform. a) SEM image showing Ag@MOF particles, b) cross-sectional SEM image showing the side view of multilayered Ag@MOF platform, and c) Scheme showing remote tracking of CO2 in real time for several cycles using multilayered Ag@MOF platform. d) Time-resolved SERS intensity profile of 1360 cm^{-1} band, showing the absorption and detection of CO_2 in several cycles. Reproduced with permission from ref. [81b]. Copyright 2019, American Chemical Society. B) Fabrication and TEM/STEM images of plasmonic-MOFs. a) Schematic procedure followed for the synthesis. b) TEM images of PS beads and AgNPs and STEM images (bright and dark field) for PS@Ag, Ag@ZIF-thin, and thick plasmonic-MOFs. c) Operando SERS spectra for the photocatalytical degradation of rhodamine B under 532 nm illumination. d) Degradartion curves for the diferent materials PS@Ag, Ag@ZIF-thin, and thick plasmonic-MOFs. Reproduced with permission from ref. [75]. Copyright 2024, Wiley VHC.

and trapping efficiency. Additionally, incorporating stimuli-responsive components, such as thermosensitive polymers or pH-tunable MOFs, would enable dynamic control over analyte capture and release, opening new possibilities for reusable or programmable SERS platforms.

Scalability remains another crucial consideration for the practical deployment of porous SERS substrates. While techniques like ice templating and colloidal crystal templating have shown promise for creating monolithic porous structures, further innovation is needed to enable large-area, cost-effective manufacturing. Moreover, standardized protocols for characterizing pore size distributions and their correlation with SERS performance must be established to facilitate meaningful comparisons across different material systems.

From an applications perspective, porous SERS substrates hold immense potential for operando studies and real-time monitoring. Their inherent molecular enrichment capabilities make them ideal for investigating catalytic processes within confined nanoreactors or tracking transient species in complex environments such as biological or environmental fluids. The development of stand-off SERS sensors based on porous plasmonic materials could also transform environmental monitoring by enabling remote detection of trace gases and pollutants. However, challenges related to long-term stability, particularly for polymer- and MOF-based substrates, and signal reproducibility across batches must be systematically addressed to ensure reliable performance under operational conditions.

Acknowledgements

The authors acknowledge financial support from the Spanish Ministerio de Ciencia e Innovación under projects (PID2023-152767NB-I00/AEI/10.13039/501100011033, PID2020-120306RB-I00/AEI/10.13039/501100011033, TED2021-132101B-I00/AEI/10.13039/501100011033, PID2020-113704RB-I00/AEI/10.13039/501100011033), Xunta de Galicia/FEDER (IN607A 2018/5 and Centro Singular de Investigación de Galicia, Acc. 2019–2022, ED431G 2019-06).

Conflict of Interest

The authors declare no conflict of interest.

Keywords

hotspots, MOFs, molecular enrichment, plasmonics, porosity, SERS

Received: April 30, 2025
Revised: July 22, 2025
Published online: August 7, 2025

[1] a) L. L. Lin, R. Alvarez-Puebla, L. M. Liz-Marzán, M. Trau, J. Wang, L. Fabris, X. Wang, G. Liu, S. Xu, X. X. Han, L. Yang, A. Shen, S. Yang, Y. Xu, C. Li, J. Huang, S.-C. Liu, J.-A. Huang, I. Srivastava, M. Li, L. Tian, L. B. T. Nguyen, X. Bi, D. Cialla-May, P. Matousek, N. Stone, R. P. Carney, W. Ji, W. Song, Z. Chen, et al., *ACS Appl. Mater. Interfaces* **2025**, *17*, 16287; b) J. Langer, D. Jimenez De Aberasturi, J. Aizpurua, R. A. Alvarez-Puebla, B. Auguié, J. J. Baumberg, G. C. Bazan, S. E. J. Bell, A. Boisen, A. G. Brolo, J. Choo, D. Cialla-May, V. Deckert, L. Fabris, K. Faulds, F. J. García De Abajo, R. Goodacre, D. Graham, A. J. Haes, C. L. Haynes, C. Huck, T. Itoh, M. Käll, J. Kneipp, N. A. Kotov, H. Kuang, E. C. Le Ru, H. K. Lee, J.-F. Li, X. Y. Ling, et al., *ACS Nano* **2020**, *14*, 28; c) C. Y. Li, Z. Q. Tian, *Chem. Soc. Rev.* **2024**, *53*, 3579; d) J. Yi, E. M. You, R. Hu, D. Y. Wu, G. K. Liu, Z. L. Yang, H. Zhang, Y. Gu, Y. H. Wang, X. Wang, H. Ma, Y. Yang, J. Y. Liu, F. R. Fan, C. Zhan, J. H. Tian, Y. Qiao, H. Wang, S. H. Luo, Z. D. Meng, B. W. Mao, J. F. Li, B. Ren, J. Aizpurua, V. A. Apkarian, P. N. Bartlett, J. Baumberg, S. E. J. Bell, A. G. Brolo, L. E. Brus, et al., *Chem. Soc. Rev.* **2024**, *54*, 1453.

[2] a) J. T. Golab, J. R. Sprague, K. T. Carron, G. C. Schatz, R. P. Van Duyne, *J. Chem. Phys.* **1988**, *88*, 7942; b) J. Kneipp, H. Kneipp, B. Wittig, K. Kneipp, *Nano Lett.* **2007**, *7*, 2819.

[3] a) A. B. Zrimsek, N. Chiang, M. Mattei, S. Zaleski, M. O. McAnally, C. T. Chapman, A. I. Henry, G. C. Schatz, R. P. Van Duyne, *Chem. Rev.* **2017**, *117*, 7583; b) R. Zhang, Y. Zhang, Z. C. Dong, S. Jiang, C. Zhang, L. G. Chen, L. Zhang, Y. Liao, J. Aizpurua, Y. Luo, J. L. Yang, J. G. Hou, *Nature* **2013**, *498*, 82.

[4] M. Liebel, I. Calderon, N. Pazos-Perez, N. F. van Hulst, R. A. Alvarez-Puebla, *Angew. Chem. Int. Ed.* **2022**, *61*, 202200072.

[5] M. Liebel, N. Pazos-Perez, N. F. van Hulst, R. A. Alvarez-Puebla, *Nat. Nanotechnol.* **2020**, *15*, 1005.

[6] a) Z. Q. Tian, B. Ren, *Annu. Rev. Phys. Chem.* **2004**, *55*, 197; b) C. Hess, *Chem. Soc. Rev.* **2021**, *50*, 3519.

[7] R. Deidda, P. Y. Sacre, M. Clavaud, L. Coïc, H. Avohou, P. Hubert, E. Ziemons, *Trends Anal. Chem.* **2019**, *114*, 251.

[8] a) G. H. Kim, J. Son, J. M. Nam, *ACS Nano* **2025**, *19*, 2992; b) I. B. Becerril-Castro, V. Salgueiriño, M. A. Correa-Duarte, R. A. Alvarez-Puebla, *Adv. Funct. Mater.* **2024**, *34*, 2314084; c) J. Mosquera, Y. Zhao, H. J. Jang, N. Xie, C. Xu, N. A. Kotov, L. M. Liz-Marzán, *Adv. Funct. Mater.* **2020**, *30*, 1902082; d) K. Yang, X. Yao, B. Liu, B. Ren, *Adv. Mater.* **2021**, *33*, 2007988.

[9] S. Yang, X. Dai, B. B. Stogin, T. S. Wong, *Proc. Natl. Acad. Sci. USA* **2015**, *113*, 268.

[10] P. Aldeanueva-Potel, E. Faoucher, R. A. Alvarez-Puebla, L. M. Liz-Marzán, M. Brust, *Anal. Chem.* **2009**, *81*, 9233.

[11] J. Plou, M. Charconnet, I. Garciá, J. Calvo, L. M. Liz-Marzán, *ACS Nano* **2021**, *15*, 8984.

[12] R. Alvarez-Puebla, L. M. Liz-Marzán, F. J. García de Abajo, *J. Phys. Chem. Lett.* **2010**, *1*, 2428.

[13] T. Zorlu, B. Puértolas, I. B. Becerril-Castro, L. Guerrini, V. Giannini, M. A. Correa-Duarte, R. A. Alvarez-Puebla, *ACS Nanosci. Au* **2023**, *3*, 222.

[14] W. Chen, S. Zhang, M. Kang, W. Liu, Z. Ou, Y. Li, Y. Zhang, Z. Guan, H. Xu, *Light Sci. Appl.* **2018**, *7*, 56.

[15] a) R. Du, X. Fan, X. Jin, R. Hübner, Y. Hu, A. Eychmüller, *Matter* **2019**, *1*, 39; b) X. Jiang, R. Du, R. Hübner, Y. Hu, A. Eychmüller, *A Matter* **2021**, *4*, 54.

[16] J. Erlebacher, M. J. Aziz, A. Karma, N. Dimitrov, K. Sieradzki, *Nature* **2001**, *410*, 450.

[17] H. Qiu, Z. Zhang, X. Huang, Y. Qu, *ChemPhysChem* **2011**, *12*, 2118.

[18] X. Xia, Y. Wang, A. Ruditskiy, Y. Xia, *Adv. Mater.* **2013**, *25*, 6313.

[19] a) K. D. Gilroy, A. Ruditskiy, H. C. Peng, D. Qin, Y. Xia, *Chem. Rev.* **2016**, *116*, 10414; b) M. Rycenga, C. M. Cobley, J. Zeng, W. Li, C. H. Moran, Q. Zhang, D. Qin, Y. Xia, *Chem. Rev.* **2011**, *111*, 3669; c) S. Kwon, M. J. Oh, S. Lee, G. Lee, I. Jung, M. Oh, S. Park, *J. Am. Chem. Soc.* **2023**, *145*, 27397.

[20] G. Bernard, C. H. P. Lupis, *Metall. Trans.* **1971**, *2*, 555.

[21] R. A. Alvarez-Puebla, D. J. Ross, G. A. Nazri, R. F. Aroca, *Langmuir* **2005**, *21*, 10504.

[22] a) R. A. Alvarez-Puebla, G. A. Nazri, R. F. Aroca, *J. Mater. Chem.* **2006**, *16*, 2921; b) R. A. Alvarez-Puebla, J. P. Bravo-Vasquez, P. Cheben, D.-X. Xu, P. Waldron, H. Fenniri, *J. Colloid Interface Sci.* **2009**, *333*, 237.

[23] M. Fleischmann, P. J. Hendra, A. J. McQuillan, *Chem. Phys. Lett.* **1974**, *26*, 163.

[24] J. Biener, A. Wittstock, L. A. Zepeda-Ruiz, M. M. Biener, V. Zielasek, D. Kramer, R. N. Viswanath, J. Weissmüller, M. Bäumer, A. V. Hamza, *Nat. Mater.* **2009**, *8*, 47.

[25] A. Mariño-López, M. Blanco-Formoso, L. N. Furini, A. Sousa-Castillo, E. Tiryaki, M. Pérez-Lorenzo, M. Testa-Anta, V. Salgueiriño, N. A. Kotov, R. A. Alvarez-Puebla, M. A. Correa-Duarte, *Langmuir* **2019**, *35*, 4110.

[26] L. Lu, A. Eychmüller, A. Kobayashi, Y. Hirano, K. Yoshida, Y. Kikkawa, K. Tawa, Y. Ozaki, *Langmuir* **2006**, *22*, 2605.

[27] D. Walsh, L. Arcelli, T. Ikoma, J. Tanaka, S. Mann, *Nat. Mater.* **2003**, *2*, 386.

[28] M. Yang, R. Alvarez-Puebla, H.-S. Kim, P. Aldeanueva-Potel, L. M. Liz-Marzán, N. A. Kotov, *Nano Lett.* **2010**, *10*, 4013.

[29] H.-L. Gao, L. Xu, F. Long, Z. Pan, Y.-X. Du, Y. Lu, J. Ge, S.-H. Yu, *Angew. Chem. Int. Ed.* **2014**, *53*, 4561.

[30] L. Qiu, J. Z. Liu, S. L. Y. Chang, Y. Wu, D. Li, *Nat. Commun.* **2012**, *3*, 1241.

[31] G. Fang, X. Lin, J. Wu, W. Xu, W. Hasi, B. Dong, *Small* **2025**, *21*, 2408670.

[32] a) L. Zhang, Y. Guo, R. Hao, Y. Shi, H. You, H. Nan, Y. Dai, D. Liu, D. Lei, J. Fang, *Nat. Commun.* **2021**, *12*, 6849. b) Y. Zheng, A. H. Soeriyadi, L. Rosa, S. H. Ng, U. Bach, J. J. Gooding, *Nat. Commun.* **2015**, *6*, 8797.

[33] a) C. Qu, Y. Li, G. Li, X. Wang, M. Su, H. Liu, *ACS Appl. Mater. Interfaces* **2024**, *16*, 32824; b) Y. Jia, S. N. Shmakov, E. Pinkhassik, *ACS Appl. Mater. Interfaces* **2016**, *8*, 19755.

[34] A. Lee, S. Dubinsky, E. Tumarkin, M. Moulin, A. A. Beharry, E. Kumacheva, *Adv. Funct. Mater.* **2011**, *21*, 1959.

[35] L. Rodríguez-Lorenzo, R. A. Álvarez-Puebla, I. Pastoriza-Santos, S. Mazzucco, O. Stéphan, M. Kociak, L. M. Liz-Marzán, F. J. García de Abajo, *J. Am. Chem. Soc.* **2009**, *131*, 4616.

[36] N. Pazos-Perez, C. S. Wagner, J. M. Romo-Herrera, L. M. Liz-Marzán, F. J. García de Abajo, A. Wittemann, A. Fery, R. A. Alvarez-Puebla, *Angew. Chem. Int. Ed.* **2012**, *51*, 12688.

[37] M. Mueller, M. Tebbe, D. V. Andreeva, M. Karg, R. A. Alvarez Puebla, N. P. Perez, A. Fery, *Langmuir* **2012**, *28*, 9168.

[38] R. A. Álvarez-Puebla, R. Contreras-Cáceres, I. Pastoriza-Santos, J. Pérez-Juste, L. M. Liz-Marzán, *Angew. Chem. Int. Ed.* **2009**, *48*, 138.

[39] X. Qian, J. Li, S. Nie, *J. Am. Chem. Soc.* **2009**, *131*, 7540.

[40] T.-M. Liu, J. Yu, C. A. Chang, A. Chiou, H. K. Chiang, Y.-C. Chuang, C.-H. Wu, C.-H. Hsu, P.-A. Chen, C.-C. Huang, *Sci. Rep.* **2014**, *4*, 5593.

[41] Y. Li, J. Luo, G. Xie, D. Zhu, C. Zhao, X. Zhang, M. Liu, Y. Wu, Y. Guo, W. Yu, *ACS Appl. Poly. Mater.* **2025**, *7*, 3406.

[42] H. Gehan, L. Fillaud, M. M. Chehimi, J. Aubard, A. Hohenau, N. Felidj, C. Mangeney, *ACS Nano* **2010**, *4*, 6491.

[43] a) R. F. Aroca, P. J. G. Goulet, D. S. Dos Santos, R. A. Alvarez-Puebla, O. N. Oliveira, *Anal. Chem.* **2005**, *77*, 378; b) D. G. Montjoy, J. H. Bahng, A. Eskafi, H. Hou, N. A. Kotov, *J. Am. Chem. Soc.* **2018**, *140*, 7835.

[44] P. Podsiadlo, M. Michel, J. Lee, E. Verploegen, N. W. Shi Kam, V. Ball, J. Lee, Y. Qi, A. J. Hart, P. T. Hammond, N. A. Kotov, *Nano Lett.* **2008**, *8*, 1762.

[45] S. Abalde-Cela, S. Ho, B. Rodríguez-González, M. A. Correa-Duarte, R. A. Álvarez-Puebla, L. M. Liz-Marzán, N. A. Kotov, *Angew. Chem. – Int. Ed.* **2009**, *48*, 5326.

[46] N. T. Tuyet, N. Félidj, C. Mangeney, *Chem. Mater.* **2016**, *28*, 3564.

[47] a) J. P. Monteiro, S. M. Predabon, S. da Cleiser Thiago Pereira, E. Radovanovic, E. M. Girotto, *J. Appl. Poly. Sci.* **2015**, *132*, 42449; b) H. I. Muri, A. Bano, D. R. Hjelme, A. Single-Point, *J. Light. Technol.* **2018**, *36*, 1159.
[48] A. Freytag, S. Sánchez-Paradinas, S. Naskar, N. Wendt, M. Colombo, G. Pugliese, J. Poppe, C. Demirci, I. Kretschmer, D. W. Bahnemann, P. Behrens, N. C. Bigall, *Angew. Chem. – Int. Ed.* **2016**, *55*, 1200.
[49] a) Z. Mu, X. Zhao, Y. Huang, M. Lu, Z. Gu, *Small* **2015**, *11*, 6036; b) G. A. Vinnacombe-Willson, C. García-Astrain, L. Troncoso-Afonso, M. Wagner, J. Langer, P. González-Callejo, D. D. Silvio, L. M. Liz-Marzán, *Chem. Mater.* **2024**, *36*, 5192.
[50] B. Miranda, R. Moretta, P. Dardano, I. Rea, C. Forestiere, L. D. Stefano, *Adv. Mater. Technol.* **2022**, *7*, 2101425.
[51] Y. A. L. Lee, Z. Mousavikhamene, A. K. Amrithanath, S. M. Neidhart, S. Krishnaswamy, G. C. Schatz, T. W. Odom, *Small* **2021**, *18*, 2103865.
[52] S. Chandna, S. Paul, R. Kaur, K. Gogde, J. Bhaumik, *ACS Appl. Poly. Mater.* **2022**, *4*, 8962.
[53] G. A. Vinnacombe-Willson, Y. Conti, S. J. Jonas, P. S. Weiss, A. Mihi, L. Scarabelli, *Adv. Mater.* **2022**, *34*, 2205330.
[54] I. B. Becerril-Castro, F. Munoz-Munoz, A. B. Castro-Ceseña, A. L. González, R. A. Alvarez-Puebla, J. M. Romo-Herrera, *Nanoscale* **2021**, *13*, 1738.
[55] A. Mariño-Lopez, A. Sousa-Castillo, M. Blanco-Formoso, L. N. Furini, L. Rodríguez-Lorenzo, N. Pazos-Perez, L. Guerrini, M. Pérez-Lorenzo, M. A. Correa-Duarte, R. A. Alvarez-Puebla, *ChemNanoMat* **2019**, *5*, 46.
[56] M. N. Sanz-Ortiz, K. Sentosun, S. Bals, L. M. Liz-Marzán, *ACS Nano* **2015**, *9*, 10489.
[57] M. Blanco-Formoso, A. Sousa-Castillo, X. Xiao, A. Mariño-Lopez, M. Turino, N. Pazos-Perez, V. Giannini, M. A. Correa-Duarte, R. A. Alvarez-Puebla, *Nanoscale* **2019**, *11*, 21872.
[58] G. Bodelón, V. Montes-García, V. López-Puente, E. H. Hill, C. Hamon, M. N. Sanz-Ortiz, S. Rodal-Cedeira, C. Costas, S. Celiksoy, I. Pérez-Juste, L. Scarabelli, A. La Porta, J. Pérez-Juste, I. Pastoriza-Santos, L. M. Liz-Marzán, *Nat. Mater.* **2016**, *15*, 1203.
[59] B. Mir-Simon, I. Reche-Perez, L. Guerrini, N. Pazos-Perez, R. A. Alvarez-Puebla, *Chem. Mater.* **2015**, *27*, 950.
[60] L. Troncoso-Afonso, G. A. Vinnacombe-Willson, C. García-Astrain, L. M. Liz-Márzan, *Chem. Soc. Rev.* **2024**, *53*, 5118.
[61] Y. Sun, D. Lou, W. Liu, Z. Zheng, X. Chen, *Adv. Opt. Mater.* **2023**, *11*, 2201549.
[62] J. Zhang, J. Liu, S. Wang, P. Zhan, Z. Wang, N. Ming, *Adv. Funct. Mater.* **2004**, *14*, 1089.
[63] a) C. Vázquez-Vázquez, B. Vaz, V. Giannini, M. Pérez-Lorenzo, R. A. Alvarez-Puebla, M. A. Correa-Duarte, *J. Am. Chem. Soc.* **2013**, *135*, 13616; b) M. Sanles-Sobrido, W. Exner, L. Rodríguez-Lorenzo, B. Rodríguez-González, M. A. Correa-Duarte, R. A. Álvarez-Puebla, L. M. Liz-Marzan, *J. Am. Chem. Soc.* **2009**, *131*, 2699.
[64] a) E. C. Le Ru, P. G. Etchegoin, *Annu. Rev. Phys. Chem.* **2012**, *63*, 65; b) P. J. G. Goulet, R. F. Aroca, *Anal. Chem.* **2007**, *79*, 2728.
[65] M. Rycenga, Z. Wang, E. Gordon, C. M. Cobley, A. G. Schwartz, C. S. Lo, Y. Xia, *Angew. Chem., Int. Ed.* **2009**, *48*, 9924.
[66] P. Riveragil, C. Vazquez-Vazquez, V. Giannini, M. P. Callao, W. J. Parak, M. A. Correa-Duarte, R. A. Alvarez-Puebla, *Angew. Chem., Int. Ed.* **2013**, *52*, 13694.
[67] a) V. López-Puente, P. C. Angelomé, G. J. A. A. Soler-Illia, L. M. Liz-Marzán, *ACS Appl. Mater. Interfaces* **2015**, *7*, 25633; b) V. López-Puente, S. Abalde-Cela, P. C. Angelomé, R. A. Alvarez-Puebla, L. M. Liz-Marzán, *J. Phys. Chem. Lett.* **2013**, *4*, 2715.
[68] Y. Negrín-Montecelo, A. Sousa-Castillo, N. Cardeñoso-Garrido, L. Guillade, L. V. Besteiro, M. Vázquez-González, R. A. Alvarez-Puebla, B. Puértolas, M. A. Correa-Duarte, *Adv. Energy Mater.* **2025**, 2501526.
[69] T. Zorlu, M. A. Correa-Duarte, R. A. Alvarez-Puebla, *J. Chem. Phys.* **2023**, *158*, 171001.
[70] D. Men, S. Feng, G. Liu, L. Hang, T. Zhang, A. Sensitive, *Part. Part. Syst. Charact.* **2020**, *37*, 1900452.
[71] a) Y. Cai, Y. Wu, T. Xuan, X. Guo, Y. Wen, H. Yang, *ACS Appl. Mater. Interfaces* **2018**, *10*, 15412; b) W. Shang, C. Zeng, Y. Du, H. Hui, X. Liang, C. Chi, K. Wang, Z. Wang, J. Tian, *Adv. Mater.* **2016**, *29*, 1604381.
[72] X. Xie, Y. Zhang, L. Zhang, J. Zheng, Y. Huang, H. Fa, *Anal. Chem.* **2021**, *93*, 13219.
[73] C. Carrillo-Carrión, R. Martínez, M. F. Navarro Poupard, B. Pelaz, E. Polo, A. Arenas-Vivo, A. Olgiati, P. Taboada, M. G. Soliman, Ú. Catalán, S. Fernández-Castillejo, R. Solà, W. J. Parak, P. Horcajada, R. A. Alvarez-Puebla, P. del Pino, *Angew. Chem. – Int. Ed.* **2019**, *58*, 7078.
[74] T. Zorlu, I. B. Becerril-Castro, B. Puertolas, V. Giannini, M. A. Correa-Duarte, R. A. Alvarez-Puebla, *Angew. Chem. – Int. Ed.* **2023**, *62*, 202305299.
[75] T. Zorlu, I. B. Becerril-Castro, A. Sousa-Castillo, B. Puértolas, L. V. Besteiro, Z. Wang, A. Govorov, M. A. Correa-Duarte, R. A. Alvarez-Puebla, *Adv. Funct. Mater.* **2024**, *34*, 2410352.
[76] F. Zhang, X. Hu, E. W. Roth, Y. Kim, S. T. Nguyen, *Chem. Mater.* **2020**, *32*, 4292.
[77] a) Z. Li, J. Liu, X. Yi, W. Wu, F. Li, Z. Zhu, H. Li, J. Shi, Y. Xu, F. Zhou, W. Liu, *Adv. Funct. Mater.* **2021**, *32*, 2109541; b) H. Ohara, S. Yamamoto, D. Kuzuhara, T. Koganezawa, H. Oikawa, M. Mitsuishi, *ACS Appl. Mater. Interfaces* **2020**, *12*, 50784.
[78] R. Patra, D. Sarma, *ACS Appl. Mater. Interfaces* **2024**, *16*, 10196.
[79] a) D. Sun, M. Xu, Y. Jiang, J. Long, Z. Li, *Small Methods* **2018**, *2*, 1800164; b) S. Sun, Y. Xiao, L. He, Y. Tong, D. Liu, J. Zhang, *ZrChemistryselect* **2020**, *5*, 13855.
[80] R. Yang, B. Zhang, Y. Wang, Y. Zheng, Q. Zhang, X. Yang, *Anal. Methods* **2023**, *15*, 4851.
[81] a) G. C. Phan-Quang, X. Han, C. S. L. Koh, H. Y. F. Sim, C. L. Lay, S. X. Leong, Y. H. Lee, N. Pazos-Perez, R. A. Alvarez-Puebla, X. Y. Ling, *Acc. Chem. Res.* **2019**, *52*, 1844; b) G. C. Phan-Quang, N. Yang, H. K. Lee, H. Y. F. Sim, C. S. L. Koh, Y. C. Kao, Z. C. Wong, E. K. M. Tan, Y. E. Miao, W. Fan, T. Liu, I. Y. Phang, X. Y. Ling, *ACS Nano* **2019**, *13*, 12090.
[82] H. Sun, S. Cong, Z. Zheng, Z. Wang, Z. Chen, Z. Zhao, *J. Am. Chem. Soc.* **2019**, *141*, 870.
[83] R. A. Alvarez-Puebla, L. M. Liz-Marzán, *Angew. Chem. – Int. Ed.* **2012**, *51*, 11214.
[84] X. Xie, N. Gao, Y. Huang, Y. Fang, *ACS Appl. Mater. Interfaces* **2022**, *14*, 51468.

Miguel A. Correa-Duarte received his degree in Chemistry from the University of Santiago de Compostela, Spain, in 1997, and his Ph.D. from the University of Vigo, Spain, in 2002. He is currently the Director of the Research Center in Nanomaterials and Biomedicine and a Full Professor at the University of Vigo. Additionally, he is a member of the Galicia Sur Health Research Institute (IISG) and the Network Centre for Biomedical Research in Mental Health (CIBERSAM). His current research interests focus on nanomaterials, particularly the synthesis and functionalization of structures such as core-shell nanohybrids, carbon nanotube-based inorganic and organic nanocomposites, and nanoreactors. These materials are developed for applications in plasmonic-based sensing and photocatalysis

Brian Becerril-Castro received his B.S. in Nanotechnology from the Universidad Nacional Autónoma de México (Mexico) in 2017. He is currently pursuing a Ph.D. at the Universitat Rovira i Virgili in Spain, where he conducts research in the Plasmonic and Ultradetection Group under the supervision of Ramon A. Alvarez-Puebla. His research centers on advanced plasmonic systems, including inkjet-printed SERS chemosensors and modular nanostructures, with the goal of developing ultrasensitive tools for chemical and biological sensing

Ramon A. Alvarez-Puebla is an ICREA Professor at the Universitat Rovira i Virgili in Tarragona. He holds a BSc in Chemistry from Universidad de Navarra and a PhD in Surface Science from Universidad Publica de Navarra, 2003. He was postdoc at University of Windsor and General Motors Corporation, worked as Research Officer at the National Institute for Nanotechnology of the National Research Council of Canada and as Associate Professor at the Universidade de Vigo. In particular, he is interested in nanophotonics, SERS and their applications in nanomedicine, chemical biology and photocatalysis.